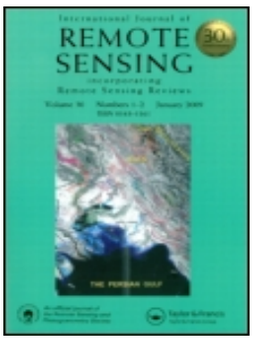

International Journal of Remote Sensing

ISSN: 0143-1161 (Print) 1366-5901 (Online) Journal homepage: https://www.tandfonline.com/loi/tres20

Characterizing fractional vegetation cover and land surface temperature based on sub-pixel fractional impervious surfaces from Landsat TM/ETM+

Youshui Zhang, Angela Harris & Heiko Balzter

To cite this article: Youshui Zhang, Angela Harris & Heiko Balzter (2015) Characterizing fractional vegetation cover and land surface temperature based on sub-pixel fractional impervious surfaces from Landsat TM/ETM+, International Journal of Remote Sensing, 36:16, 4213-4232, DOI: 10.1080/01431161.2015.1079344

To link to this article: https://doi.org/10.1080/01431161.2015.1079344

International Journal of Remote Sensing, 2015
Vol. 36, No. 16, 4213–4232, http://dx.doi.org/10.1080/01431161.2015.1079344

Taylor & Francis
Taylor & Francis Group

Characterizing fractional vegetation cover and land surface temperature based on sub-pixel fractional impervious surfaces from Landsat TM/ETM+

Youshui Zhang[a,b]*, Angela Harris[a], and Heiko Balzter[c,d]

[a]*School of Environment and Development, University of Manchester, Manchester M13 9PL, UK;* [b]*College of Geography, Fujian Normal University, Fuzhou 350007, P.R. China;* [c]*Centre for Landscape and Climate Research, University of Leicester, Leicester LE1 7RH, UK;* [d]*National Centre for Earth Observation, University of Leicester, Leicester LE1 7RH, UK*

(*Received 24 January 2015; accepted 23 July 2015*)

Estimating the distribution of impervious surfaces and vegetation is important for analysing urban landscapes and their thermal environment. The application of a crisp classification of land-cover types to analyse urban landscape patterns and land surface temperature (LST) in detail presents a challenge, mainly due to the complex characteristics of urban landscapes. In this article, sub-pixel percentage impervious surface areas (ISAs) and fractional vegetation cover (FVC) were extracted from bitemporal Thematic Mapper/Enhanced Thematic Mapper Plus (TM/ETM+) data by linear spectral mixture analysis (LSMA). Their accuracy was assessed with proportional area estimates of the impervious surface and vegetation extracted from high-resolution data. A range approach was used to classify percentage ISA into different categories by setting thresholds of fractional values and these were compared for their LST patterns. For each ISA category, FVC, LST, and percentage ISA were used to quantify the urban thermal characteristics of different developed areas in the city of Fuzhou, China. Urban LST scenarios in different seasons and ISA categories were simulated to analyse the seasonal variations and the impact of urban landscape pattern changes on the thermal environment. The results show that FVC and LST based on percentage ISA can be used to quantitatively analyse the process of urban expansion and its impacts on the spatial–temporal distribution patterns of the urban thermal environment. This analysis can support urban planning by providing knowledge on the climate adaptation potential of specific urban spatial patterns.

1. Introduction

The urban heat island (UHI) effect is caused by increased use of impervious surface materials with low specific capacity, and an associated decrease in vegetation cover and water pervious surfaces leading to rising land surface temperature (LST); as well as the emission of heat from human activities (Kato and Yamaguchi 2005, 2007). Increases in impervious surface areas (ISAs) have significant environmental implications, including the reduction in evapotranspiration, more rapid surface runoff, increased storage and transfer of sensible heat, and a deterioration in air and water quality (Owen, Carlson, and Gillies 1998; Chen et al. 2006). These changes have a significant influence on human health, landscape aesthetics, and the local urban environment (Mcpherson et al. 1997; Xian and Crane 2006). Clarification as to how changes in the coverage of impervious

*Corresponding author. Email: zhangyoushui@sina.com

surfaces and vegetation cover contribute to observed variations in local urban LST is required in order to aid mitigation of the UHI effect and enable urban areas to effectively adapt to climate change.

LST is a physical parameter that is influenced by land surface–atmosphere interactions and energy fluxes between the land surface and the atmosphere (Wan and Dozier 1996). Accurate information on landscape patterns and LST is critical to environmental monitoring, urban planning, and management. Advances in remote sensing have enabled the extensive use of satellite remote sensing to estimate LST at global and local scales (e.g. Justice et al. 1998; Chen et al. 2006). Data from the Landsat suite of satellites (e.g. Thematic Mapper (TM) and Enhanced Thematic Mapper (ETM+)) are often used to detect spatial and temporal variations in urban ISA, vegetation, and surface temperature, mainly due to a combination of their relatively high spatial resolution (30 m for visible and near infrared bands, and 120 or 60 m for the thermal infrared band for TM and ETM+, respectively) and their ease of access (Woodcock and Strahler 1987; Zhang, Odeh, and Han 2009).

The abundance of vegetation and ISAs are often used as indicators of urban climate (Lo, Quattrochi, and Luvall 1997; Gallo and Owen 1999; Yuan and Bauer 2007; Xian and Crane 2006; Xu, Lin, and Tang 2013). The fractional vegetation cover (FVC) in urban areas can be related to the normalized difference vegetation index (NDVI) through a simple, yet not necessarily linear, transformation (e.g. Nemani and Running 1989; Lo, Quattrochi, and Luvall 1997; Gallo and Owen 1999; Weng, Lu, and Schubring 2004; Yuan and Bauer 2007; Zhang, Odeh, and Han 2009; Karnieli et al. 2010; Sandholt, Rasmussen, and Andersen 2002). Consequently, the FVC is also closely linked to LST and is therefore one of the most important variables in land surface modelling (Zhang, Odeh, and Ramadan 2013). However, in comparison to the use of NDVI for the estimation of FVC, the measurement of impervious surfaces is more desirable since they are more stable and not affected by seasonal changes (Arnold and Gibbons 1996; Civco et al. 2002). Consequently, ISA is a useful additional metric for an analytical understanding of LST anomalies.

The heterogeneity of urban landscapes is such that traditional per-pixel classifiers, such as the maximum likelihood classifier, cannot effectively handle the mixed-pixel problem of remotely sensed imagery. This hampers an accurate analysis of the spatial structure of urban environments. Sub-pixel or soft classification approaches provide a good way to characterize and quantify the heterogeneity present in urban land-cover patterns (Lu and Weng 2006; Frazier and Wang 2011; Weng 2012). Linear spectral mixture (LSM) models, such as the vegetation–impervious–soil (VIS) model, assume that the spectral signature of land cover in urban environments is a linear combination of vegetation, impervious surface, and soil, if water surfaces are ignored (Ridd 1995). Such models are often used to map the fractional cover of urban landscapes on a continuous scale (e.g. Smith et al. 1990; Rashed 2008; Michishita, Jiang, and Xu 2012). Information on the percentage ISA and vegetation cover can provide a complementary metric to the traditionally applied NDVI or crisp land-cover classes for LST and UHI analysis (Weng, Lu, and Schubring 2004). The different urban land-cover/land-use patterns can be defined by different percentage ISA categories to reveal various densities and patterns of urban development. A number of studies have used vegetation fractional cover and ISA as a means to analyse the spatio-temporal patterns of LST (Gillies and Carlson 1995; Weng, Lu, and Schubring 2004; Xian and Crane 2006; Yuan and Bauer 2007; Zhang, Odeh, and Han 2009, 2013). In these studies, percentage ISA and FVC were extracted from remotely sensed data and individually analysed with LST. To our knowledge, no current published

research has calculated FVC values based on discrete categories of percentage ISA and analysed its effect on urban LST. By investigating the relationships between the mean LST and FVC based on different percentage ISA categories, our aim was to characterize these relationships of urban landscape patterns and thermal characteristics more accurately.

The surface UHI is obviously influenced by seasonal variation (Roth, Oke, and Emery 1989; Voogt and Oke 2003). Although the temporal change trends between the LST and percentage ISA show some seasonal differences, in general there is a linear relationship between LST and percentage ISA in different seasons when urban expansion is considered (Yuan and Bauer 2007; Zhang, Odeh, and Han 2009). However, with increased concerns about local impacts of global climate change and urban expansion, it is necessary to differentiate the seasonal variation from impacts of urban expansion on the urban thermal environment. Such an analysis has the power to indicate spatio-temporal patterns of both the urban thermal environment and urban expansion, and to develop future urban climate scenarios under urban expansion. This will be helpful for strategic planning and urban design that explicitly considers adaptation to unavoidable climate change.

The main aim of this study is to quantify the spatial–temporal patterns of different impervious surface areas and their influence on urban LST in Fuzhou, China. Sub-pixel fractional cover will be derived through linear spectral unmixing and the fractional values of ISA will subsequently be divided to create a series of ISA coverage categories in relation to the density of urban development using the range approach. Based on the different ISA categories, urban thermal patterns will be analysed by remotely sensing mean FVC and mean LST, and quantifying the impacts of seasonal variations and urban landscape pattern changes on LST.

2. Study area and remotely sensed data

Fuzhou City is the capital city of Fujian province and is located on the southeast coast of China (Figure 1). The population of Fuzhou has been rapidly increasing since the 1980s,

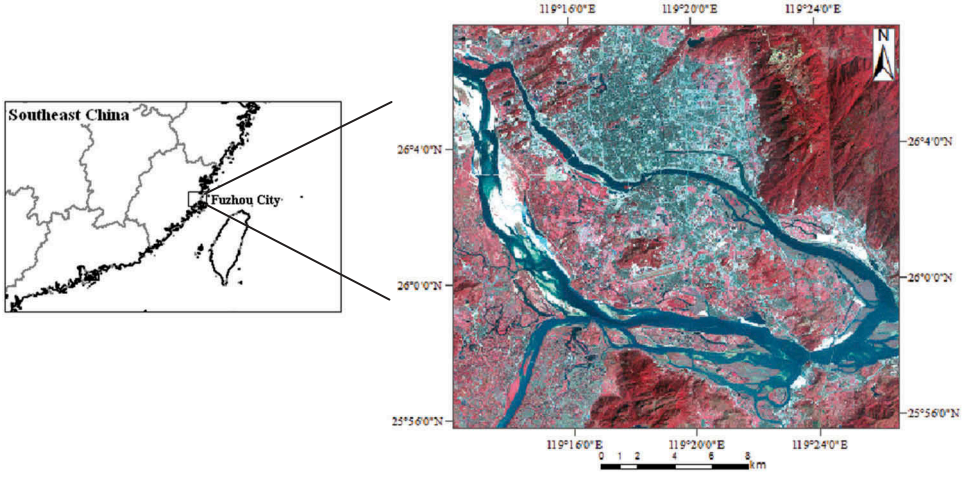

Figure 1. Location of the study area; the figure on the right shows a false colour composite Landsat ETM+ image, acquired on 4 March 2001 (red, band 4; green, band 3; blue, band 2).

Table 1. Landsat and high-resolution images of Fuzhou used in the study.

Sensor data	Acquisition date	Spectral and special resolutions
TM	15 June 1989	Three visible bands (blue, green, and red), one near infrared (NIR) band, and two shortwave infrared (SWIR) bands with 30 m spatial resolution, one thermal band with 120 m spatial resolution
ETM+	4 March 2001	The same as TM, but the thermal band with 60 m spatial resolution
IKONOS	29 October 2000	Three visible bands (blue, green, and red) and one near infrared (NIR) band with 4 m spatial resolution
Aerial photographs	20 May 1988	Panchromatic photograph (black/white), the scale is 1:25000 (approximately 2 m spatial resolution)

with a permanent population of approximately 5.2 million in 1989 and 6.5 million in 2001. The city is on a subtropical plain sandwiched between the Gu and Qi mountains. The vegetation cover in the region is predominantly evergreen and the FVC in different seasons is almost invariable. The increase in population, coupled with the high summer temperatures (average of 37.5 days per year with a temperature >35°C) and mild winters, makes the city an ideal study area.

The climatic variations of Fuzhou during spring, autumn, and winter are small compared to summer. Therefore, bitemporal (early spring and summer) Landsat images, together with a high-resolution IKONOS image and aerial photograph, were used in this research (Table 1). All data were georeferenced to a common Universal Transverse Mercator (UTM) coordinate system based on the geocoded high-resolution IKONOS image and the aerial photograph. The root mean square error (RMSE) of the georectification of the Landsat data was <0.3 pixels (<9 m).

The visible and near infrared bands of the Landsat images were converted to surface reflectance using the Second Simulation of the Satellite Signal in the Solar Spectrum (6S) radiative transfer code (Schroeder et al. 2006). The NDVI was calculated based on surface reflectance of bands 3 and 4. The IKONOS image and the aerial photograph were used to extract land-cover types to analyse the accuracy of fractional covers extracted from the Landsat data.

3. Methods

3.1. Land surface temperature retrieval

The thermal band of the Landsat imagery was first converted to top-of-atmosphere (TOA) radiance (L_λ, mW cm^{-2} sr^{-1}) using sensor-specific gains and offsets (Chander and Markham 2003; Schroeder et al. 2006). The TOA radiance of the thermal infrared band was then converted to surface-leaving radiance using the radiative transfer code Moderate Resolution Atmospheric Transmission (MODTRAN) 4.1 to estimate atmospheric transmission, upwelling, and downwelling radiance. Surface-leaving radiance L_T was subsequently calculated using Equation (1) (Barsi et al. 2005; Berk et al. 1999):

$$L_T = (L_\lambda - L_u - \tau(1-\varepsilon)L_d)/\tau\varepsilon, \quad (1)$$

where L_T, L_u, and L_d are surface-leaving radiance of kinetic temperature, upwelling (atmospheric path radiance), and downwelling (sky radiance), respectively; and τ is the atmospheric transmission and ε is the emissivity of the surface. Here, ε was derived from land-cover types and NDVI (e.g. Sobrino et al. 2001; Yuan and Bauer 2007; Van De Grienzd and Owe 1993; Zhang, Wang, and Li 2006). In Equation (1), L_λ is the TOA radiance image at wavelength λ with 120 m resolution for TM band 6 and 60 m resolution for ETM+ band 6. The ε parameter was calculated from 30 m resolution land-cover data and an associated NDVI image. L_u, L_d, and τ are scalars. Therefore, Equation (1) is a process of merging 120/60 m resolution L_λ and 30 m resolution ε images, the resolution of L_T is thus 30 m.

In the final step, radiance (L_T) was converted to surface temperature using the Landsat specific estimate of the Planck curve (Equation (2)) (Chander and Markham 2003):

$$T = K_2/\ln(K_1/L_T + 1), \tag{2}$$

where T is the temperature in kelvin (K), K_1 is the pre-launch calibration constant in W m^{-2} sr^{-1} μm^{-1}, and K_2 is another pre-launch calibration constant in kelvin. For Landsat 5 TM, K_1 = 607.76 W m^{-2} sr^{-1} μm^{-1} and K_2 = 1260.56 K; for Landsat 7 ETM+, K_i = 666.09 W m^{-2} sr^{-1} μm^{-1} and K_2 = 1282.71 K.

3.2. Derivation of urban coverage of ISA and FVC

Linear spectral mixture analysis (LSMA) was used to extract fractional land cover from the Landsat imagery. LSMA is a sub-pixel mapping approach which assumes that the spectrum measured by a sensor is a linear combination of the spectra of all endmembers within the pixel, and that the spectral proportions of the endmembers represent proportions of the area covered by distinct features on the ground (Adams et al. 1995; Mustard and Sunshine 1999; Mitraka et al. 2012). A constrained least-squares solution, where fractions of a pixel must sum to 1 and all fractions must be greater than or equal to zero, was applied to spectrally unmix the six Landsat bands.

Endmember selection is a critical step in the use of LSMA (Boardman and Kruse 2011). In this study, image endmembers identifying spectrally pure pixels were derived by the pixel purity index (PPI) and the extremes of the image feature space. A minimum noise fraction (MNF) transformation was initially applied to the imagery to reduce inherent noise. In applying the PPI analysis to the MNF output to rank the pixels based on relative purity and spectral extremity, the PPI was computed by repeatedly projecting n-dimensional scatter plots on a random unit vector and the algorithm records the extreme pixels in each projection and the total number of times each pixel was marked as extreme. By setting a PPI threshold, the region of interest (ROI) of pure pixels was determined. Within this ROI, endmember classes were selected by choosing pixels at the edges of the point cloud in three-dimensional scatter plots as pure pixels. All LSMA procedures were undertaken in the environment for visualizing images 4.5.

The urban environment can be assumed to consist of four fundamental components: water, vegetation, impervious surfaces, and soil (Ridd 1995). Because of the varied spectral response of many urban environments, two endmembers were used to represent the difference in albedo of impervious surfaces, i.e. high and low (Lu and Weng 2006). Because the water endmember class is not directly relevant to urban land-cover composition, and the spectral features of water are similar to those of low-albedo impervious areas, water was masked from the images and not included as an endmember. Consequently,

four endmembers were defined in the study area: vegetation, high-albedo impervious surfaces, low-albedo impervious surfaces, and soil. The high-albedo impervious surfaces are mainly the bright impervious surfaces with high spectral reflectance (such as concrete); and the low-albedo impervious surfaces are mainly the dark impervious surfaces with low spectral reflectance (such as asphalt).

Initial results indicated some confusion between bright high-albedo ISAs and bare soil areas distributed alongside the river. Field investigation showed that the bare soil (fine sand) is mainly distributed along the river. Land-cover thematic data, extracted from an IKONOS image and aerial photographs, were used to identify these regions and their values were set to zero in the high-albedo fraction images. The high-albedo and low-albedo impervious surfaces were subsequently summed to create an overall percentage cover of ISA.

3.3. *Accuracy assessment of percentage ISA and vegetation cover derivation*

Accuracy assessment of fractional images is inherently difficult. Due to a lack of *in situ* fractional data, the accuracy of the fractional land-cover maps was assessed using high-resolution IKONOS imagery and aerial photographs as validation data. The characteristic scale of urban reflectance has been shown to be between 10 and 20 m (Small 2003, 2005), thus we assumed that the majority of pixels within the high-resolution images were spectrally homogeneous.

The TM/ETM+ images were georeferenced to a common UTM coordinate system based on the rectified high-resolution IKONOS image and aerial photographs. The RMSE of rectification is less than 0.3 pixels (9 m). The iterative self-organizing data analysis technique algorithm (ISODATA) was used to map ISAs and vegetation cover from the reference imagery (IKONOS imagery and aerial photographs). The percentage cover of ISA and vegetation was determined for each 30 × 30 m Landsat pixel and compared with the LSMA fractional images. This approach was deemed feasible because the two dates for which the aerial photographs and IKONOS images were acquired were close to those of the Landsat imagery. Because the high-resolution imagery did not cover the entire study area, the test area of Figure 2 was selected as

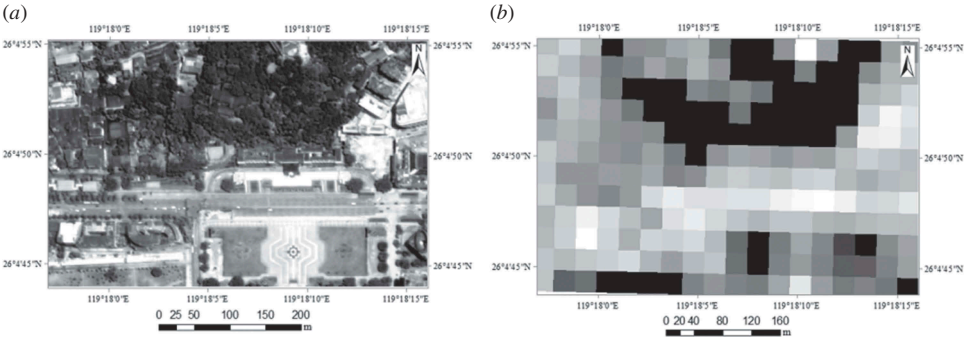

Figure 2. A comparison of urban land-cover pattern in the same position between auxiliary IKONOS imagery (*a*) and percentage ISA extracted from the ETM+ imagery by LSMA (*b*), illustrating the light colour ISA and deep colour vegetation in the high-resolution imagery and the corresponding percentage ISA from 0% to 100% extracted from the mixed pixels from relatively coarse spatial resolution data.

an example (180 TM/ETM+ pixels) to derive the scatter plots to analyse the accuracy of the sub-pixel fractional covers.

Percentage cover of ISA and vegetation derived from the reference data were determined for each 30 × 30 m Landsat pixel and then compared with the LSMA fractional images. Scatter plots of fractional ISA and vegetation coverage were used to determine the accuracy of the LSMA at the level of the individual pixel. The accuracy was also assessed for test areas within the imagery by comparing the areas of the cumulative fractional coverage of impervious surfaces and vegetation with those estimated from the high-resolution reference imagery. Using the high-resolution data as surrogate 'ground truth', the accuracy was assessed by comparing the areas of accumulated impervious surfaces and vegetation generated from the TM/ETM+ imagery by LSMA with the areas extracted from high-resolution data. Test areas were chosen to avoid temporal land-cover change influencing the accuracy assessment, in which the land-cover type was unlikely to have changed because the aerial photographs and IKONOS images were, respectively, acquired nearly on the same date as the TM/ETM+ imagery.

3.4. Creation of fractional ISA categories by the range approach

In order to quantify urban land-cover patterns and their relationship with the thermal environment, percentage ISA cover was classified into categories representing different levels of urban development. A range approach was used to group pixels based on proportional ranges of fractional values. For each endmember fractional image, each pixel was assigned to one of 10 equal categories (0–10%, 10–20%, 20–30%, …, 90–100%) depending on its fractional value. Grouping fractional covers in this manner facilitates analysis of observed urban LSTs within each zone in detail, and the spatial distribution patterns of the urban thermal environment can be analysed and compared in areas of different urban density.

4. Results and discussion

4.1. Accuracy of fractional cover maps

4.1.1 Per-pixel accuracy

One sample plot (Figure 2), which overlapped with the reference data availability, was selected to derive scatter plots to assess the per-pixel accuracy of the fractional cover maps. Figure 3 shows a significant relationship ($p < 0.01$) between the fractional coverage estimates obtained from LSMA of the Landsat data and that derived from the high-resolution reference data. As shown in Figure 3, the unmixing percentage ISA and FVC by LSMA tend to have a higher error when the reference fractions are either very low or very high; slightly overestimating impervious surface fraction in less developed areas (<30% ISA) (Figures 3(*a*) and (*c*)), while overestimating and underestimating impervious surface fractions in developed areas (>60% ISA) (to some extent, inverse to FVC). Because the ISA and vegetation extracted from IKONOS and aerial photographs are the results of a crisp classification, the aggregated 30 m scale fractional cover from high-resolution data can account for the variation in spectral signatures more effectively than those extracted from the Landsat imagery by LSMA. However, in general, the unmixing results from the Landsat imagery were correlated with those from high-resolution data.

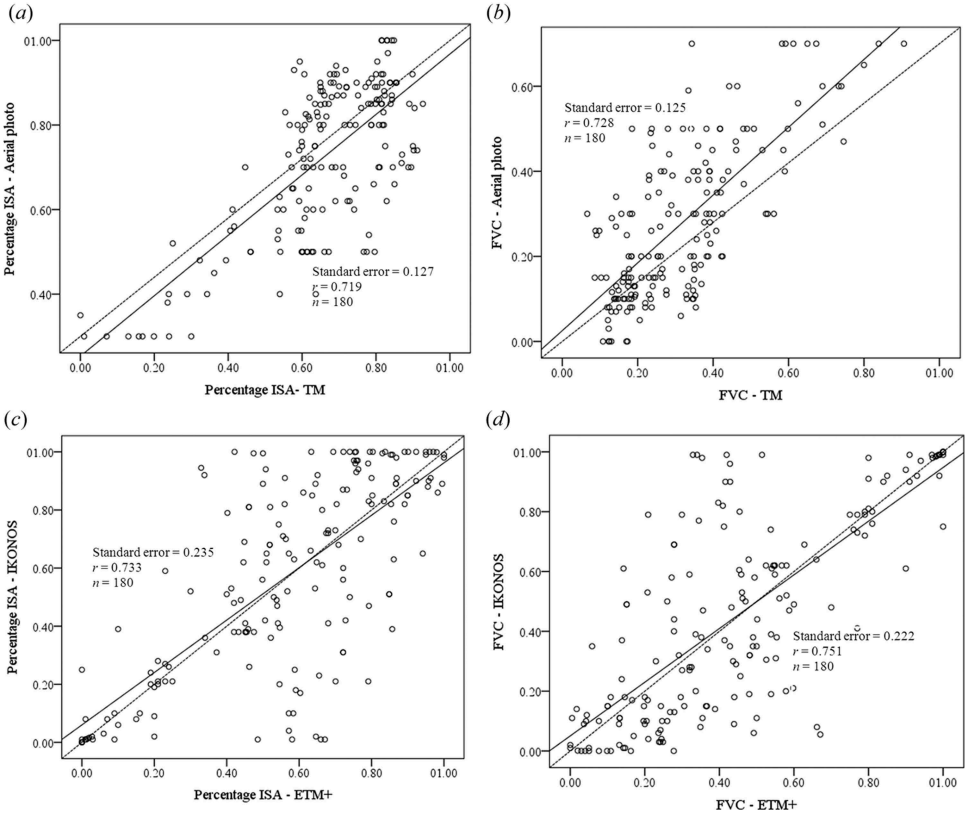

Figure 3. The scatter plots of ISA and vegetation endmember fractions unmixed from the TM/ETM+ imagery and fractional cover from high-resolution data ($p = 0.01$).

4.1.2 *Area-based accuracy*

The accuracy of the total areas of the test sites were also assessed for four locations within the imagery (Figure 4(*a*)) by comparing the cumulative area of fractional cover for each land cover with those estimated from the high-resolution reference imagery. Table 2 shows the results from a comparison of the 'reference' areal coverage obtained from IKONOS and aerial photographs, with the corresponding area calculated from the accumulation of the fractions that were obtained from the TM/ETM+ imagery by LSMA.

Table 2 indicates good agreement for ISA and vegetation between the measures calculated from the Landsat and the high-resolution imagery. The area of ISA and vegetation in the four test sites in 1989 and 2001 showed only small differences when compared with the reference data. One reason for the differences is the differences in the spatial scale that land-cover mapping can require different approaches and classification schemes at different spatial resolutions (Woodcock and Strahler 1987). For example, at a 2.5 m resolution, a land-cover class of 'tarmac' may have to be defined to map road surfaces, while at 30 m resolution, road surfaces would be located in mixed pixels with other urban land-cover classes and may be subsumed into a class 'urban areas'. The accuracy of impervious surfaces and

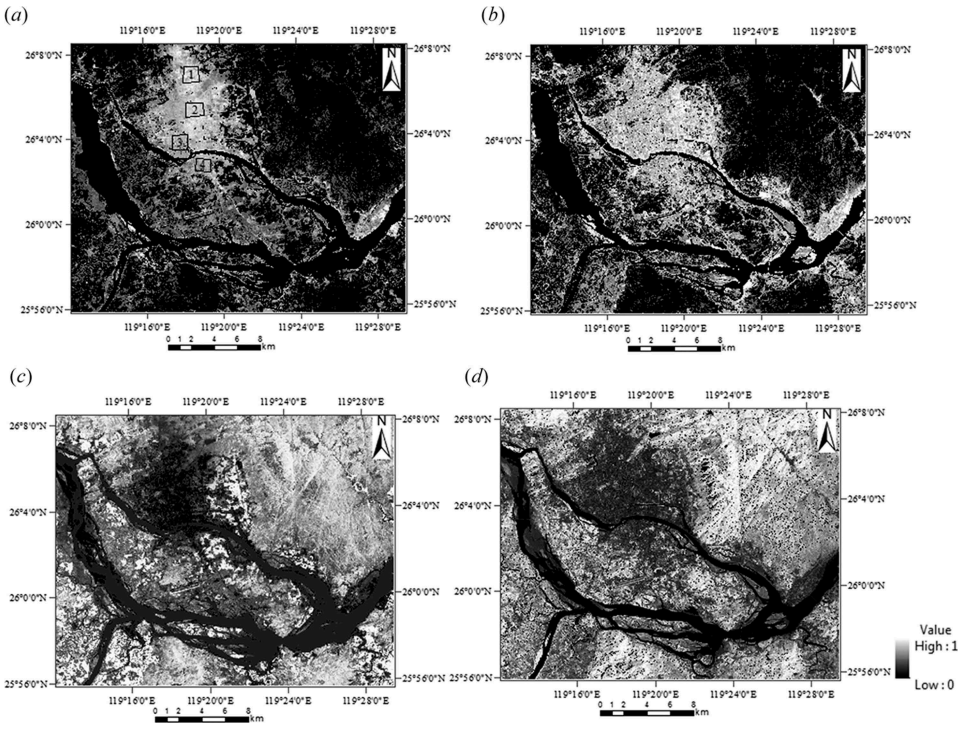

Figure 4. Fractional ISA and FVC images for six TM/ETM+ reflective bands using LSMA: (*a*) 1989 percentage ISA, (*b*) 2001 percentage ISA, (*c*) 1989 FVC, and (*d*) 2001 FVC. The four sample plots delineated with polygons in (*a*) represent test sites used for accuracy assessment. Brighter areas indicate a higher fractional abundance of the endmember.

vegetation fractions was slightly lower in 1989, which can also be seen in Figure 3. One reason for this is that the interpretation of aerial photographs and the TM images, respectively, is less precise than that of IKONOS and ETM+ because the qualities of IKONOS and ETM+ images are higher than that of the aerial photographs and the TM image in the study area. In addition, urban expansion and vegetation changes between 1989 and 2001 can also be seen from the test areas in Table 2. Because urban green spaces attracted more and more attention in urban planning, the vegetation areas of the urban test site 2 increased from 0.191 km^2 in 1989 to 0.220 km^2 in 2001. However, in general, because of urban expansion, the vegetation area decreased during this period.

4.2. Bitemporal patterns of fractional cover

Fractional covers with continuous values can be used to reveal not only the spatial structure of urban land-cover patterns, but also the change patterns in different urban categories or within-class change (Zhang, Odeh, and Han 2009). In some areas, minor land-cover change may take place at the sub-pixel scale but would not yet be detectable at the pixel scale using hard classification approaches. Figure 4 shows the results from the LSMA of the Landsat data for the years 1989 and 2001. The fractional images provide a

Table 2. Results of accuracy assessment of LSMA fractions.

	Area (km^2) from the TM image in 1989		Area (km^2) from aerial photographs in 1988		Average difference (%)		Area (km^2) from the ETM+ image in 2001		Area (km^2) from the IKONOS image in 2000		Average difference (%)	
ISA sites	ISA	Vegetation	ISA	Vegetation	ISA	Vegetation	ISA	Vegetation	ISA	Vegetation	ISA	Vegetation
Site 1	1.570	0.508	1.662	0.499	–5.9	1.77	1.675	0.403	1.587	0.408	5.25	–1.24
Site 2	1.712	0.191	1.865	0.213	–8.9	–11.52	1.683	0.220	1.766	0.231	–4.93	–5.0
Site 3	1.224	0.555	1.396	0.592	–14.0	–6.67	1.297	0.482	1.467	0.473	–13.1	1.87
Site 4	0.963	0.435	1.034	0.403	–7.4	7.36	1.169	0.229	1.321	0.234	–13.0	–2.18
Total	5.469	1.689	5.957	1.707	–8.9	–1.06	5.824	1.334	6.141	0.346	–5.4	0.90

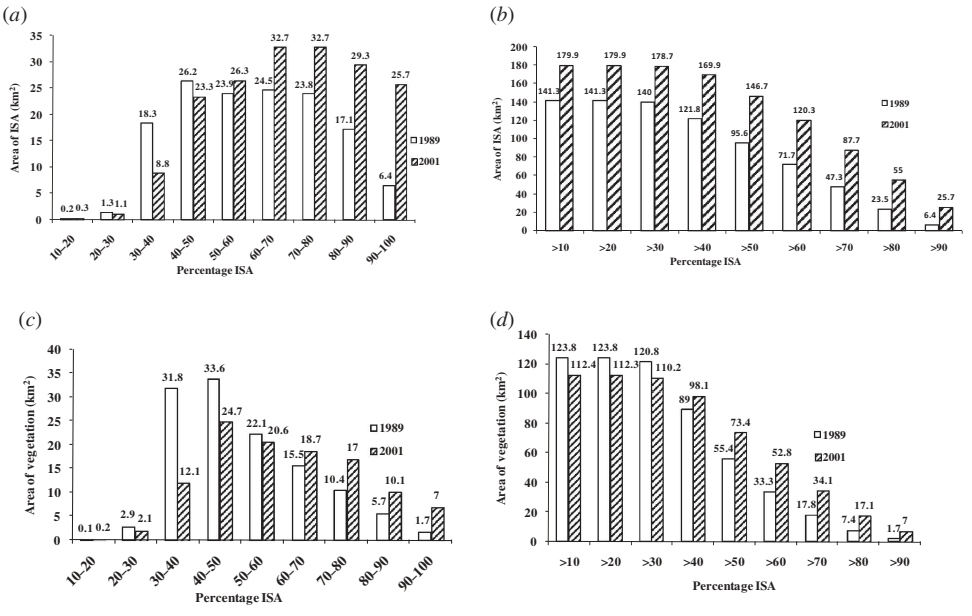

Figure 5. The total areas of ISA and vegetation (km^2) of each category of fractional cover between 1989 and 2000. (*a*) Areas of ISA for the range approach; (*b*) areas of ISA for the threshold continuum approach; (*c*) areas of vegetation for the range approach; and (*d*) areas of vegetation for the threshold continuum approach.

measure of the physical properties of the urban land-cover patterns within the scene on two different dates, thus help revealing the changing patterns of urban land-cover composition. ISA and vegetation cover vary remarkably between the core of the city and its periphery. The impervious surface area increases at the periphery of the city due to urban expansion (Figures 4(*a*) and (*b*)). The total area of urban ISA in 1989 was less than in 2001 because of urban expansion. However, the percentage coverage of ISA within some pixels was higher. One reason for this is the greater attention to the ecological planning of the urban landscape post 1989 in the study area, which may have resulted in more vegetation cover interspersed within the developed areas, as observed in Figures 4(*c*) and (*d*).

In addition to the range approach, the threshold continuum approach was also used to partition the percentage ISA using a gradient. This method only uses a lower boundary to define each zonal threshold for the categories, which was set in increments of 10% (>10%, >20%, >30%, …, >90%). For each zonal threshold, all pixels exceeding that threshold were assigned to that zone representing the degree of urban expansion. Using this approach, fractional coverage data were each grouped into nine discrete classes, one for each of the nine cover zones. Figure 5 shows the changes in impervious surfaces and vegetation areas at different percentage ISA categories classified by the range and threshold continuum approaches. The areal coverage of impervious surface/vegetation for each ISA zone was calculated by summing the total area of each pixel within that category. The area of impervious surface/vegetation in each pixel was calculated by multiplying the fractional value with the pixel area of 900 m^2, and then the total area was accumulated by the area of each pixel in the percentage ISA category. Between 1989 and 2001, impervious surface area (i.e. >10% cover) in the region increased from 141 to 180 km^2

(Figure 5(*b*)), indicating significant urban expansion over this time period. Increases in the extent of impervious surfaces were the greatest in the highest cover categories (i.e. 60–70% ISA, 70–80% ISA, 80–90% ISA, and 90–100% ISA) but decreased in the regions of 20–30%, 30–40%, and 40–50% ISA. The main reason for the decrease is that the urban development changed the 20–30%, 30–40%, and 40–50% ISA in 1989 into the >60% ISA category in 2001. This shows that the urbanization mainly took place in the >60% ISA category. The greatest increase in the area of impervious surfaces occurred in the 90–100% ISA zone (6.4 and 25.7 km^2 in 1989 and 2001, respectively), indicating that high-density urban development was the dominant mode of urbanization during this time period. The area variations in the categories of 0–10%, 10–20%, and 20–30% ISA (<30% ISA) were small (Figure 4(*a*)), which can also been seen in Figure 4(*b*). The areas of impervious surfaces within the threshold continuum zones decreased as the threshold increased.

The results also indicate a concurrent increase in urban fractional vegetation cover between 1989 and 2001. In order to further verify the impervious surface change and analyse the change in urban land-cover patterns, vegetation cover is also used to quantitatively characterize the urbanization patterns. Figures 5(*c*) and (*d*) show the area of vegetation based on different categories of percentage ISA between 1989 and 2001. Comparing the areas of impervious surfaces in Figures 5(*a*) and (*b*), it is observed that the area of urban vegetation (Figures 5(*c*) and (*d*)) increased in a similar manner to that of impervious surface area in the categories of 60–70% ISA, 70–80% ISA, 80–90% ISA, and 90–100% ISA (>60% ISA), suggesting that the increased urbanization during this time period was accompanied by urban greening since 1990s. Vegetation covered landscapes in urban areas were more interspersed with the various developed urban structures in 2001 in comparison to in 1989 as a result of paying more attention to urban greening as urban expansion continued. Vegetation was planted in areas such as parks, residential areas, and roadsides. Between 1989 and 2001, vegetation area decreased in coverage zones containing pixels with less than 60% ISA categories. Especially, the area of vegetation in the category of 0–10% ISA decreased from 254 km^2 in 1989 to 182 km^2 in 2001 because of urban expansion in the periphery of urban vegetation (Figure 4). The areas of impervious surfaces (Figure 5(*a*)) and vegetation (Figure 5(*c*)) all decreased in the categories of 20–30% ISA, 30–40% ISA, and 40–50% ISA between two dates. However, in the category of 50–60% ISA, the area of impervious surfaces slightly increased from 1989 to 2001, the area of the vegetation slightly decreased.

A comparison of the range and threshold continuum approaches for characterizing fractional coverage showed differences in both the number and the distribution of the pixels at each threshold value. For the range approach, the number of pixels in each of the ranges is relatively small and the pixels are comparatively uniform. For the threshold continuum approach, all pixels above a threshold value are cumulative, and a larger number of pixels are included as the threshold decreases. Consequently, we can infer that the range approach is suitable for analysis on specific ranges of land cover such as different urban development density areas in this study with comparative uniform pixels. The specific land-cover patterns and the changes can be quantified through range threshold. The threshold continuum method results in heterogeneous pixels (especially for a low threshold) and is more suitable for characterizing the landscape with a continuum of values such as the degree of urban expansion. In some situations, it may be necessary to combine these two approaches to analyse the spatial patterns of specific ranges and their impacts on the entire area or the thermal environment of the whole area. This information is important for urban planning.

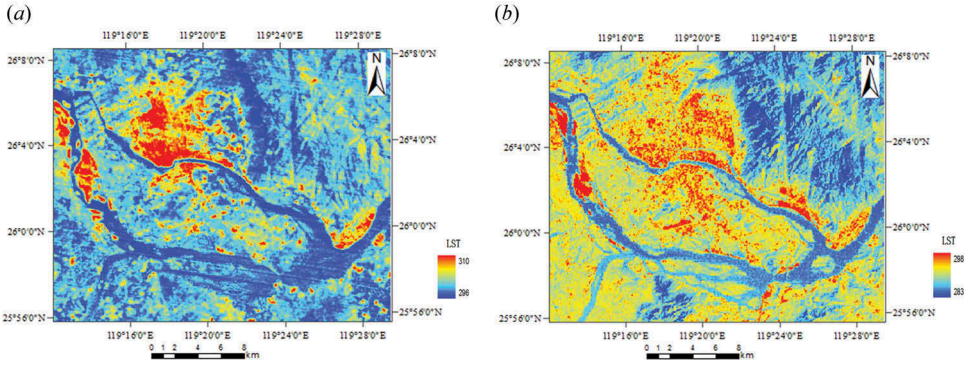

Figure 6. Spatial distribution patterns of land surface temperature (LST) from the TM image acquired on 15 June 1989 (*a*) and ETM+ image acquired on 4 March 2001 (*b*).

4.3. Seasonal impact on LST in different percentage ISA categories

Impervious surfaces and vegetation cover are two of the primary urban land covers. Quantification of the relationship between these land covers and LST will help to facilitate the characterization of spatial patterns of urban LST and provide useful information for urban ecological planning. Figure 6 shows the spatial patterns of LST across Fuzhou City in the imagery obtained in 1989 and 2001. LST appears to be stratified by the degree of imperviousness and vegetation cover, with higher LST occurring over more developed land.

The LST varies with urban landscape patterns, changing urban expansion and seasonal variations. In order to quantify the urban thermal environment for urban climate adaptation, it is necessary to differentiate the impact of urban expansion on LST within each percentage ISA category from the impact of seasonal variations. Because of the limitation of the TM/ETM+ data acquisitions, we could not acquire all the seasonal data in 1998 and 2001. However, the climatic variations of Fuzhou during spring, autumn, and winter are small compared to summer. Therefore, bitemporal (early spring and summer) Landsat images are applicable to analyse the impact of urban expansion and seasonal variations on LST in this research. What is more, due to the seasonality and the variability of atmospheric conditions, it is inappropriate to directly compare LST values between two dates. However, by simulating LST scenarios, we can determine how seasonal variations and urban landscape pattern changes have an impact on urban LST in a quantitative manner.

As discussed by Zhang, Odeh, and Han (2009), although the relationships between percentage ISA and mean LST may be different in each season, a relatively strong linear relationship between the mean LST and percentage ISA was observed in the study area in both 1989 and 2001. The regression equation of the mean LST and the mean percentage ISA in summer (June 15) in 1989 is:

$$y = 0.017x + 299.61\left(R^2 = 0.6945\right). \tag{3}$$

For early spring (March 4) in 2001, the regression equation is:

$$y = 0.0191x + 288.66\left(R^2 = 0.6731\right). \tag{4}$$

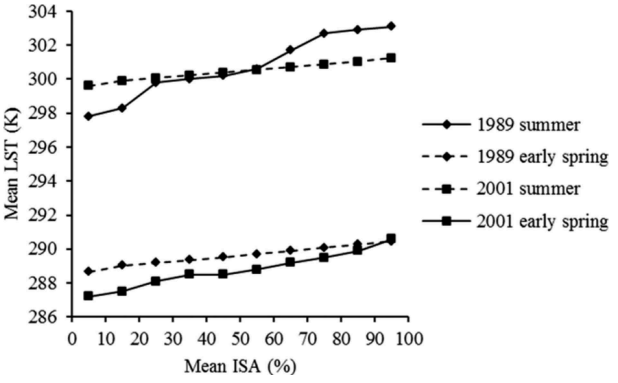

Figure 7. The relationship between the mean LST and the mean ISA for different ISA categories in summer and early spring for both dates of study.

Here, y and x are the mean LST and the mean percentage ISA, respectively. Based on this analysis, LST scenarios can be created in different seasons to analyse the seasonal impact on LST.

Figure 7 shows the mean LST and percentage ISA in summer and early spring of 1989 and 2001. In which, the mean LST scenarios in 1989 in early spring were calculated based on the mean percentage ISA and Equation (4) (here, x in Equation (4) is percentage ISA values in 1989). Similarly, the mean LST scenarios of 2001 in summer were calculated based on the mean percentage ISA and Equation (3) (x in Equation (3) is percentage ISA values in 2001). Through comparing LST in different years and with LST scenarios, we can differentiate LST change from urban expansion and seasonal variations.

The results show that although urban expansion impacted on the variations of LST within each ISA category, the primary reason for LST variations between 1989 and 2001 is seasonal variation. By comparing the mean LST in two seasons, the seasonal LST difference for each percentage ISA category can be quantified. In Figure 7, the LST is on average 9–12 K higher for each percentage ISA category in the summer of 1989 than the simulated LST for early spring of 1989. Similarly, simulated LST for the summer of 2001 is approximately 11–12 K higher than the LST in the early spring of 2001. In general, the seasonal variation between early spring and summer changed the LST by about 10–12 K in the urban landscape patterns with >10% ISA.

Comparing the expected LST for the same season and the same climatic conditions in different years, the urban landscape patterns changed in each percentage ISA category from 1989 to 2001. The distributions and the shapes of ISA changed, and the areas of ISA subtly changed because of urban expansion, which also resulted in subtle variations of the mean percentage ISA values and the mean LST in each ISA category in the two years. In the study area, the LST differences by the ISA category are within about 2 K in summer between 1989 and 2001 and about 1 K in early spring between 1989 and 2001. Although the accuracies of simulating LST are lower than those obtained from direct calculation from TM/ETM+ data, and the simulated LST has a smaller range than the LST from TM/ETM+, the results show that the simulated LST scenarios can be used to quantify the seasonal variations and impacts of urban landscape pattern change on the spatio-temporal patterns of LST in different percentage ISA categories.

For urban planning and adaptation to climate change, an analysis and prediction of LST scenarios for different seasons and different percentage ISA categories are needed to explore the climate adaptation potential in different percentage ISA categories of cities. This can be achieved through the characterization of the study site using the analytical method shown here, and quantifying the city's thermal environmental functions under urban expansion and different climate scenarios.

4.4. *FVC and LST analysis in different percentage ISA categories*

At the pixel scale, LST increases as the coverage of impervious urban area expands and decreases as the vegetation coverage increases. Measuring LST, using the fractional variation in impervious surfaces and vegetation in the pixels of a particular percentage ISA category, can not only provide precise characterization of urban land cover and LST patterns, but may also be useful for urban ecological planning.

In contrast to previous published studies, our approach goes beyond a simple analysis of FVC and its impact on LST. Here, FVC is analysed in a stratified design by the percentage ISA category. Figure 8 illustrates the differences in the mean LST and FVC for each percentage ISA category. Natural landscapes are depicted by low ISA but high FVC. The dense natural vegetation reduces the surface radiant temperature leading to relatively low LST values because vegetation reduces the surface radiant temperature through evapotranspiration (Zhang, Odeh, and Ramadan 2013). The results show that the average FVC gradually decreases with a concomitant increase in LST, and high average FVC lowers the mean LST for both years.

As shown in Figure 8, the mean LST was 301.7 K at 60–70% ISA and 300.6 K at 50–60% ISA in 1989, and 289.2 K at 60–70% ISA and 288.8 K at 50–60% ISA in 2001. The mean FVC was 31.4% at 60–70% ISA and 40.8% at 50–60% ISA in 1989, and 34.6% at 60–70% ISA and 40.2% at 50–60% ISA in 2001, respectively. Therefore, when the mean FVC increased from 31.4% to 40.8% in 1989, it lowered the mean LST by 1.1 K (LST difference between 60–70% ISA and 50–60% ISA). However, when the mean FVC increased from 34.6% to 40.2% in 2001, it only lowered the mean LST by 0.4 K, due to the seasonal differences. FVC thus has a seasonally specific cooling effect on the urban environment that depends on the evapotranspiration rate and ambient LST. Other categories can also be analysed in the same way described here. A quantification of the variation of FVC and LST in

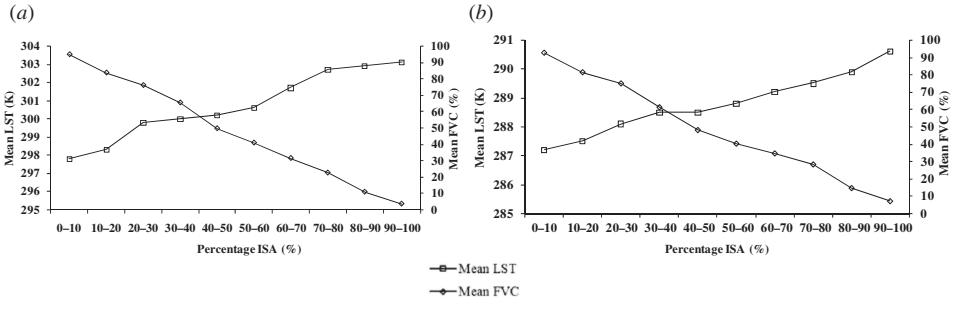

Figure 8. Mean LST and mean FVC for different ISA categories. (*a*) 15 June 1989 and (*b*) 4 March 2001.

different ISA categories can provide information on urban landscapes and their thermal environmental structure in urban areas of different degrees of development. The basis of these relationships is that higher levels of latent heat fluxes are more representative of vegetation cover in comparison to impervious surface areas where low surface moisture availability but significant sensible heat exchange occurs. With the percentage ISA maps from the TM/ETM+ and high-resolution imagery, it is possible to further analyse the spatial–temporal distribution of LST in different land-cover patterns such as transport infrastructure areas, industrial land, and residential areas of different local micro-climatic zones.

5. Conclusions

Urban expansion in Fuzhou resulted in an increase of impervious surface area and a decrease of vegetation area, which impacted on the variation in the urban thermal environment and caused changes in regional climate. Hard (per-pixel) classification of urban land-cover types cannot effectively handle the mixed pixel problem in medium spatial resolution images, commonly resulting in an underestimation or overestimation of land-cover types, especially in a complex urban land-cover pattern where impervious surfaces or vegetation account for a small proportion of the study area (Lu, Moran, and Hetrick 2011). The use of sub-pixel fractional cover can effectively interpret spatial–temporal urban land-cover and LST patterns.

In this study, LSMA was used to extract the sub-pixel percentage coverage of ISA and FVC, and the accuracy of fractional cover was assessed using test areas and correlation analysis with information obtained from very high-resolution remotely sensed imagery as reference data. The scatter plot analysis showed that the unmixing results obtained from the Landsat imagery were generally correlated with those obtained from high-resolution data. There was also good agreement between the area of ISA and vegetation between the measures calculated from the Landsat and the high-resolution imagery. The sub-pixel fractional ISA values were subsequently classified into different categories of urban developed areas using the range approach and further analysed in conjunction with LST patterns. Besides the urban landscape changes that resulted from urban expansion, seasonal variations impacted on the observed LST patterns on the two acquisition dates. LST scenarios in the ISA categories and different seasons were simulated to analyse the impacts of seasonal variation and urban landscape changes on the urban thermal environment. The results show that the presented methodology is suitable to integrate fractional cover components and LST for an investigation of the urban thermal environment. This has the advantage of characterizing urban landscape patterns and LST in different urban developed areas. Such analysis can provide knowledge for urban planning, ecological construction, and climate adaptation policies in cities.

The above results suggest three major conclusions:

(1) Classifying continuous percentage ISA into different categories, calculating FVC and LST based on the categories of percentage ISA, is a suitable approach for quantifying the process of urban expansion and its impacts on the spatial–temporal distribution patterns of the urban thermal environment.
(2) The range approach is suitable for the specific ranges of land cover with uniform pixels related to the different urban development areas. The threshold continuum approach is suitable for characterizing the landscape related to the degree of urban

expansion. The combinations of range and threshold continuum approaches are suitable for analysing complex urban land-cover patterns, urban planning, and the impact of each ISA category of the range approach on the thermal environment.

(3) LST scenarios at each percentage ISA category can be simulated in different seasons and can be used to differentiate urban landscape changes from seasonal variations on LST patterns. This methodology can also be used to predict the likely impact of urban expansion on urban climates and further provide information for urban adaptation to climate change.

The proposed methodology can add a new perspective to the understanding of urban land-cover patterns and the thermal environment. In this study, mean LST and FVC were calculated based on the 10% increments of percentage ISA. Future research can investigate the impact of utilizing different thresholds to classify percentage ISA coverage to determine whether optimal thresholds for landscape characterization can be identified in urban areas. If coarse threshold increments are applied, some inherent sub-pixel details will be lost. Although fine threshold can reveal the detailed urban land-cover pattern, it cannot effectively analyse different categories of urban developed areas and the thermal environment.

The size, shape, and spatial arrangement of the land-cover patches influence the thermal environment (Liu and Weng 2008). However, landscape metrics have not been calculated from urban fractional cover such as percentage ISA, which is closely related to urban landscape patterns. This is because these metrics cannot be calculated directly from the soft classification of ISA of remotely sensed images. Future research can discretise percentage ISA of different zones and further calculate landscape metrics to quantify the process of urban expansion and characterizing their urban thermal patterns.

Disclosure statement

No potential conflict of interest was reported by the authors.

Funding

This research was supported by a grant from the China Scholarship Council (CSC) [No. 201208350005]. Heiko Balzter was supported by the Royal Society Wolfson Research Merit Award [2011/R3].

References

Adams, J. B., D. E. Sabol, V. Kapos, R. A. Filho, D. A. Roberts, M. O. Smith, and A. Gillespie. 1995. "Classification of Multispectral Images Based on Fractions of Endmembers: Application to Land Cover Change in the Brazilian Amazon." *Remote Sensing of Environment* 52: 137–154. doi:10.1016/0034-4257(94)00098-8.

Arnold, Jr., C. L., and C. J. Gibbons. 1996. "Impervious Surface Coverage: The Emergence of a Key Environmental Indicator." *Journal of the American Planning Association* 62: 243−258. doi:10.1080/01944369608975688.

Barsi, J. A., J. R. Schott, F. D. Palluconi, and S. J. Hook. 2005. "Validation of a Web-Based Atmospheric Correction Tool for Single Thermal Band Instruments." In *Proceedings of SPIE, Earth Observing Systems X*. Vol. 5882, edited by J. J. Butler, Paper 58820E, Bellingham, WA: SPIE.

Berk, A., G. P. Anderson, P. K. Acharya, J. H. Chetwynd, L. S. Bernstein, E. P. Shettle, M. W. Matthew, and S. M. Adler-Golden. 1999. *MODTRAN4 User's Manual*, 10–35. North Andover, MA: Air Force Research Laboratory.

Boardman, J. W., and F. A. Kruse. 2011. "Analysis of Imaging Spectrometer Data Using N-Dimensional Geometry and a Mixture-Tuned Matched Filtering Approach." *IEEE Transactions on Geoscience and Remote Sensing* 49 (11): 4138–4152.

Chander, G., and B. Markham. 2003. "Revised Landsat-5 TM Radiometric Calibration Procedures and Post Calibration Dynamic Ranges." *IEEE Transactions on Geoscience and Remote Sensing* 41: 2674–2677. doi:10.1109/TGRS.2003.818464.

Chen, X. L., M. Z. Zhao, P. X. Li, Z. Y. Yin. 2006. "Remote Sensing Image-Based Analysis of the Relationship Between Urban Heat Island and Land Use/Cover Changes." *Remote Sensing of Environment* 104: 133–146. doi:10.1016/j.rse.2005.11.016.

Civco, D. L., J. D. Hurd, E. H. Wilson, C. L. Arnold, and M. P. Prisloe. 2002. "Quantifying and Describing Urbanizing Landscapes in the Northeast United States." *Photogrammetric Engineering and Remote Sensing* 68: 1083–1090.

Frazier, A. E., and L. Wang. 2011. "Characterizing Spatial Patterns of Invasive Species Using Sub-Pixel Classifications." *Remote Sensing of Environment* 115: 1997−2007. doi:10.1016/j.rse.2011.04.002.

Gallo, K. P., and T. W. Owen. 1999. "Satellite Based Adjustments for the Urban Heat Island Temperature Bias." *Journal of Applied Meteorology* 38: 806–813. doi:10.1175/1520-0450(1999)038<0806:SBAFTU>2.0.CO;2.

Gillies, R. R., and T. N. Carlson. 1995. "Thermal Remote Sensing of Surface Soil Water Content with Partial Vegetation Cover for Incorporation into Climate Models." *Journal of Applied Meteorology* 34: 745–756. doi:10.1175/1520-0450(1995)034<0745:TRSOSS>2.0.CO;2.

Justice, C., E. Vermote, J. Townshend, R. Defries, D. P. Roy, D. K. Hall, V. V. Salomonson, J. L. Privette, G. Riggs, A. Strahler, W. Lucht, R. B. Myneni, Y. Knyazikhin, S. W. Running, R. R. Nemani, Z. Wan, A. R. Huete, W. Van Leeuwen, R. E. Wolfe, L. Giglio, J. Muller, P. Lewis, and M. J. Barnsley. 1998. "The Moderate Resolution Imaging Spectroradiometer (MODIS): Land Remote Sensing for Global Change Research." *IEEE Transactions on Geoscience and Remote Sensing* 36: 1228–1249. doi:10.1109/36.701075.

Karnieli, A., N. Agam, R. Pinker, M. Anderson, M. L. Imhoff, G. G. Gutman, N. Panov, and A. Goldberg. 2010. "Use of NDVI and Land Surface Temperature for Drought Assessment: Merits and Limitations." *Journal of Climate* 23: 618–633. doi:10.1175/2009JCLI2900.1.

Kato, S., and Y. Yamaguchi. 2005. "Analysis of Urban Heat-Island Effect Using ASTER and ETM+ Data: Separation of Anthropogenic Heat Discharge and Natural Heat Radiation from Sensible Heat Flux." *Remote Sensing of Environment* 99: 44−54. doi:10.1016/j.rse.2005.04.026.

Kato, S., and Y. Yamaguchi. 2007. "Estimation of Storage Heat Flux in an Urban Area Using ASTER Data." *Remote Sensing of Environment* 110: 1–17. doi:10.1016/j.rse.2007.02.011.

Liu, H., and Q. Weng. 2008. "Seasonal Variations in the Relationship between Landscape Pattern and Land Surface Temperature in Indianapolis, USA." *Environmental Monitoring and Assessment* 144: 199–219. doi:10.1007/s10661-007-9979-5.

Lo, C. P., D. A. Quattrochi, and J. C. Luvall. 1997. "Application of High Resolution Thermal Infrared Remote Sensing and GIS to Assess the Urban Heat Island Effect." *International Journal of Remote Sensing* 18: 287–304. doi:10.1080/014311697219079.

Lu, D., E. Moran, and S. Hetrick. 2011. "Detection of Impervious Surface Change with Multitemporal Landsat Images in an Urban–Rural Frontier." *ISPRS Journal of Photogrammetry and Remote Sensing* 66: 298–306. doi:10.1016/j.isprsjprs.2010.10.010.

Lu, D., and Q. Weng. 2006. "Use of Impervious Surface in Urban Land-Use Classification." *Remote Sensing of Environment* 102: 146−160. doi:10.1016/j.rse.2006.02.010.

McPherson, E. G., D. Nowak, G. Heisler, S. Grimmond, C. Souch, R. Grant, R. Rowntree. 1997. "Quantifying Urban Forest Structure, Function, and Value, the Chicago Urban Forest Climate Project." *Urban Ecosystems* 1: 49–61. doi:10.1023/A:1014350822458.

Michishita, R., Z. Jiang, and B. Xu. 2012. "Monitoring Two Decades of Urbanization in the Poyang Lake Area, China through Spectral Unmixing." *Remote Sensing of Environment* 117: 3–18. doi:10.1016/j.rse.2011.06.021.

Mitraka, Z., N. Chrysoulakis, Y. Kamarianakis, P. Partsinevelos, and A. Tsouchlaraki. 2012. "Improving the Estimation of Urban Surface Emissivity Based on Sub-Pixel Classification of High Resolution Satellite Imagery." *Remote Sensing of Environment* 117: 125–134. doi:10.1016/j.rse.2011.06.025.

Mustard, J. F., and J. M. Sunshine. 1999. "Spectral Analysis for Earth Science: Investigations Using Remote Sensing Data." In *Remote Sensing for the Earth Sciences: Manual of Remote Sensing*. 3rd ed. Vol. 3, edited by A. N. Rencz, 251–307. New York, NY: John Wiley & Sons.

Nemani, R. R., and S. W. Running. 1989. "Estimation of Regional Surface Resistance to Evapotranspiration from NDVI and Thermal-Ir AVHRR Data." *Journal of Applied Meteorology* 28: 276–284. doi:10.1175/1520-0450(1989)028<0276:EORSRT>2.0.CO;2.

Owen, T. W., T. N. Carlson, and R. R. Gillies. 1998. "An Assessment of Satellite Remotely Sensed Land Cover Parameters in Quantitatively Describing the Climatic Effect of Urbanization." *International Journal of Remote Sensing* 19: 1663–1681. doi:10.1080/014311698215171.

Rashed, T. 2008. "Remote Sensing of Within-Class Change in Urban Neighborhood Structures." *Computers, Environment and Urban Systems* 32: 343–354. doi:10.1016/j.compenvurbsys.2008.06.007.

Ridd, M. K. 1995. "Exploring a V-I-S (Vegetation-Impervious Surface-Soil) Model for Urban Ecosystem Analysis through Remote Sensing: Comparative Anatomy for Cities." *International Journal of Remote Sensing* 16: 2165–2185. doi:10.1080/01431169508954549.

Roth, M., T. R. Oke, and W. J. Emery. 1989. "Satellite-Derived Urban Heat Islands from Three Coastal Cities and the Utilization of Such Data in Urban Climatology." *International Journal of Remote Sensing* 10: 1699–1720. doi:10.1080/01431168908904002.

Sandholt, I., K. Rasmussen, and J. Andersen. 2002. "A Simple Interpretation of the Surface Temperature/Vegetation Index Space for Assessment of Surface Moisture Status." *Remote Sensing of Environment* 79: 213–224. doi:10.1016/S0034-4257(01)00274-7.

Schroeder, T. A., W. B. Cohen, C. Song, M. J. Canty, and Z. Yang. 2006. "Radiometric Correction of Multi-Temporal Landsat Data for Characterization of Early Successional Forest Patterns in Western Oregon." *Remote Sensing of Environment* 103: 16–26. doi:10.1016/j.rse.2006.03.008.

Small, C. 2003. "High Spatial Resolution Spectral Mixture Analysis of Urban Reflectance." *Remote Sensing of Environment* 88: 170–186. doi:10.1016/j.rse.2003.04.008.

Small, C. 2005. "A Global Analysis of Urban Reflectance." *International Journal of Remote Sensing* 26 (4): 661–681. doi:10.1080/01431160310001654950.

Smith, M. O., S. L. Ustin, J. B. Adams, and A. R. Gillespie. 1990. "Vegetation in Deserts: I. A Regional Measure of Abundance from Multispectral Images." *Remote Sensing of Environment* 31: 1−26. doi:10.1016/0034-4257(90)90074-V.

Sobrino, J. A., N. Raissouni, and Z. Li. 2001. "A Comparative Study of Land Surface Emissivity Retrieval from NOAA Data." *Remote Sensing of Environment* 75: 256–266. doi:10.1016/S0034-4257(00)00171-1.

Van De Grienzd, A. A., and M. Owe. 1993. "On the Relationship between Thermal Emissivity and the Normalized Difference Vegetation Index for Natural Surfaces." *International Journal of Remote Sensing* 14: 1119–1131. doi:10.1080/01431169308904400.

Voogt, J. A., and T. R. Oke. 2003. "Thermal Remote Sensing of Urban Climates." *Remote Sensing of Environment* 86: 370–384. doi:10.1016/S0034-4257(03)00079-8.

Wan, Z., and J. Dozier. 1996. "A Generalized Split-Window Algorithm for Retrieving Land-Surface Temperature from Space." *IEEE Transactions on Geoscience and Remote Sensing* 34: 892–905. doi:10.1109/36.508406.

Weng, Q. 2012. "Remote Sensing of Impervious Surfaces in the Urban Areas: Requirements, Methods, and Trends." *Remote Sensing of Environment* 117: 34–49. doi:10.1016/j.rse.2011.02.030.

Weng, Q., D. Lu, and J. Schubring. 2004. "Estimation of Land Surface Temperature-Vegetation Abundance Relationship for Urban Heat Island Studies." *Remote Sensing of Environment* 89: 467–483. doi:10.1016/j.rse.2003.11.005.

Woodcock, C. E., and A. H. Strahler. 1987. "The Factor of Scale in Remote Sensing." *Remote Sensing of Environment* 21: 311–332. doi:10.1016/0034-4257(87)90015-0.

Xian, G., and M. Crane. 2006. "An Analysis of Urban Thermal Characteristics and Associated Land Cover in Tampa Bay and Las Vegas Using Landsat Satellite Data." *Remote Sensing of Environment* 104: 147–156. doi:10.1016/j.rse.2005.09.023.

Xu, H., D. Lin, and F. Tang. 2013. "The Impact of Impervious Surface Development on Land Surface Temperature in a Subtropical City: Xiamen, China." *International Journal of Climatology* 33: 1873–1883. doi:10.1002/joc.2013.33.issue-8.

Yuan, F., and M. E. Bauer. 2007. "Comparison of Impervious Surface Area and Normalized Difference Vegetation Index as Indicators of Surface Urban Heat Island Effects in Landsat Imagery." *Remote Sensing of Environment* 106: 375–386. doi:10.1016/j.rse.2006.09.003.

Zhang, J., Y. Wang, and Y. Li. 2006. "A C++ Program for Retrieving Land Surface Temperature from the Data of Landsat TM/ETM+ Band6." *Computers & Geosciences* 32: 1796–1805. doi:10.1016/j.cageo.2006.05.001.

Zhang, Y., I. Odeh, and C. Han. 2009. "Bi-Temporal Characterization of Land Surface Temperature in Relation to Impervious Surface Area, NDVI and NDBI, Using a Sub-Pixel Image Analysis." *International Journal of Applied Earth Observation and Geoinformation* 11: 256–264. doi:10.1016/j.jag.2009.03.001.

Zhang, Y., I. Odeh, and E. Ramadan. 2013. "Assessment of Land Surface Temperature in Relation to Landscape Metrics and Fractional Vegetation Cover in an Urban/Peri-Urban Region Using Landsat Data." *International Journal of Remote Sensing* 34: 168–189. doi:10.1080/01431161.2012.712227.